Chapter 13
Applications of Remote Sensing for Flood Inundation Mapping at Urban Areas in MENA Region: Case Studies of Five Egyptian Cities

Karim I. Abdrabo, Mohamed Saber, Sameh A. Kantoush, Tamer ElGharbawi, Tetsuya Sumi, and Bahaa Elboshy

Abstarct This chapter focuses on using various remote sensing data for monitoring floods and developing risk maps. It covers a wide range of issues, reviews remote sensing data types, processing techniques, and discussing the limitations and challenges of using remote sensing images in flood monitoring, especially in MENA region. Furthermore, the chapter presents a number of previous attempts of flood monitoring in the MENA region clarifying the data they depend on and the extent of reaching reliable results. The main aim of this chapter is to highlight the role of the available remote sensing data remotely sensed, including optical data, multispectral data, and Synthetic Aperture Radar (SAR) data in supporting flood-related research and investigation such as monitoring and mapping flood events and risk where is the lacking the observational data at the arid regions.

Keywords Satellite-based data · Flood inundation mapping · MENA region · Optical · SAR · Remotely sensed data · Urban area

K. I. Abdrabo (✉)
Faculty of Urban and Regional Planning, Cairo University, Giza, Egypt

Department of Urban Management, Graduate School of Engineering, Kyoto University, Kyoto, Japan
e-mail: m.karim.ibrahim@cu.edu.eg

M. Saber · S. A. Kantoush · T. Sumi
Disaster Prevention Research Institute (DPRI), Kyoto University, Kyoto, Japan
e-mail: mohamedmd.saber.3u@kyoto-u.ac.jp; kantoush.samehahmed.2n@kyoto-u.ac.jp; sumi.tetsuya.2s@kyoto-u.ac.jp

T. ElGharbawi
Department of Civil Engineering, Suez Canal University, Ismailia, Egypt

B. Elboshy
Architectural Engineering Department, Faculty of Engineering, Tanta University, Tanta, Egypt
e-mail: bahaa.elboshi@f-eng.tanta.edu.eg

M. M. Al Saud (ed.), *Applications of Space Techniques on the Natural Hazards in the MENA Region*, https://doi.org/10.1007/978-3-030-88874-9_13

13.1 Introduction

The United Nations (UNISDR, 2015) pointed out that 43% of natural disasters that occurred globally from 1995 to 2015 were water-related disasters, affecting more than half (56%) of all people. The socioeconomic effects correlated with floods are recorded and documented in the developed and developing countries (Bisht et al., 2018; Martín-Vide & Llasat, 2018; Ozturk et al., 2018). Moreover, according to the International Disaster Database (EM-DAT; www.em-dat.be), floods are the most frequent disaster with the highest impact in terms of the number of people affected. Flash floods cause the devastating impacts; however, it is more severe in developing countries such as MENA region. During the past few decades, the frequencies of extreme events have increased in the Middle Eastern North African (MENA) Region (Zhang et al., 2005). The Arab region is characterized by increasing the frequency and intensity of extreme storm events which resulting in devastating flash floods, along with drought threats (Abdrabo et al., 2020a; Saber et al., 2020; Saber & Habib, 2016). This might be attributed to climate change or human impacts; however, the reasons are still not well understood. In spite of the multiple evidence and the growing awareness of the flood risks, the modeling capacity of flood dynamics remains poor, which is mainly related to the availability of data. Flash flood risk mitigation requires precise and accurate flood monitoring measures for helping hazard management (Arora et al., 2020). One of such measures is mapping the inundation areas, which is considered as one of the main concerns among scientists and governments around the globe (Ali et al., 2019, 2020). Flood inundation maps are used mainly for (1) Forecast scenarios; (2) Mitigation and planning – flood risk analyses (3) Timely response; (4) Damage assessment; and (5) Environmental and ecological assessments. Flood inundation mapping are generally difficult and considered more difficult in MENA region due to the difficulty of accessing the affected areas, that consequently affect the performance of the hydrological modeling which requires a detailed observational dataset for calibration and validation (Abdrabo et al., 2020b; Abushandi & Merkel, 2011; Hall et al., 2014; Kilpatrick & Cobb, 1985; Lin, 1999; Pilgrim et al., 1988; Rodier & Roche, 1978:197; Wheater et al., 2007).

In this context, Remote Sensing (RS) is an extremely useful source of observation data that could overcome the decline in field surveys and observational stations, especially in MENA region. RS plays an important role in all the phases of flood hazard management, from preparedness, emergency management, and civil protection phases and up to damage assessment for flood risk reduction. RS data provide huge advantages: low costs, data acquisition reliability, overcoming the local difficulties such as site accessibility etc. Moreover, it can play a key role in the calibration and validation of hydrological and hydraulic models in addition to providing real-time flood mapping and monitoring applications (Domeneghetti et al., 2019; Haq et al., 2012). Although the number of state-of-the-art and innovative research studies in these areas is increasing, the full potential of RS in enhancing flood mapping, modeling, and prediction has not been exploited (Saber et al., 2010;

Sanyal & Lu, 2004; University of Waterloo et al., 1993). However, as is often the case, new opportunities and applications pose new challenges: the nature of the data, the different size, and scale of the objects and the processes which can be now investigated, even the sheer quantity of available data, all require new or more powerful tools to be suitably dealt with.

RS primarily in the form of satellite and airborne imagery and altimetry such as (Resurs-P, GeoEye, and WorldView, or from drones). The different uses of RS products in the case of flood monitoring are as follows: (1) elevation data such as Shuttle Radar Topography Mission (SRTM) and digital elevation model (DEM) from WorldView-2 stereo pair imagery; (2) The land use/land cover and soil properties which can be obtained from fused ASTER multispectral and ALOS-PALSAR Synthetic Aperture Radar (SAR) data; (3) Rainfall products such as the Tropical Rainfall Measuring Mission (TRMM) (Kummerow et al., 1998) (Chen et al., 2015; Kneis et al., 2014; Ochoa et al., 2014; Prasetia et al., 2013), the Climate Prediction Centre morphing method (CMORPH) from NOAA CPC (Joyce et al., 2004), (PERSIANN) from the University of California (Hsu et al., 1997; Yoshimoto & Amarnath, 2017), Global Satellite Mapping of Precipitation (GSMaP) from Japan Science and Technology Agency (JST) and Japan Aerospace Exploration Agency (JAXA), IMERG LATE, and IMERG EARLY from NASA which are two new rainfall data products. There are many other remotely sensed meteorological products that are publicly available and occasionally updated with ground-based information, are commonly known as global datasets. Utilizing such high-resolution, multi-temporal data give the chance to enhance the performances of the forecast, alert, and post-event monitoring of inundation events (Refice et al., 2018b). The integration of remotely sensed data (such as Data Terrain Models (DTMs), flood extent, river width, land cover, water level, etc.) with flood modeling significantly enhances the prediction results (Haq et al., 2012; Refice et al., 2018a). Although the previous studies showed encouraging results using different types of RS data combined with in-situ data, many challenges face such applications from an uncertain point of view.

In the present chapter, we will start with an overview of flood monitoring systems and remote sensing approaches, followed by the potential and limitations of open satellite data for flood mapping. Finally, we present some applications of remote sensing on flash floods in MENA region at five Egyptian cities.

13.2 Overview of Remote Sensing Approaches Used in Flood Monitoring

Flood monitoring activities can be divided into three sets, according to the stage of operations with respect to the event occurrence. (1) Forecast scenarios; (2) Timely response and Emergency monitoring; (3) Damage assessment (Hutter, 2006). According to each activity, the type of RS approaches and data used in each activity is determined. Forecasts rely mainly on meteorological information, so low- to medium-resolution optical data are usually implicated. In emergency monitoring,

the emphasis is clearly on fast response and relatively high resolution, so a potentially wide variety of sensors can be involved, working in both the optical and microwave spectral regions. The third type of application is the one that involves the most advanced processing techniques to defining the spatial and temporal changes of factors, which, in return, control flood generation and risk. Multi-temporal and multisensory data allow a temporal and spatial reconstruction of flood inundation, from the beginning until the end when all the inundated areas return dry.

Remote Sensing data is produced through two main components: the sensors and the platform on which the sensor is installed. There are three types of platform, surface platforms such as ladder and tall building, Arial platforms such as aircraft and balloons; and spaceborne platforms are mainly satellites and space shuttles (Liang et al., 2012).

For the sensors, there are two types of sensors, passive and active. Passive sensors detect natural radiation that is emitted or reflected by the observed object. Reflected sunlight is the most common reflect radiation and is sensed by passive sensors. Typical passive sensors include three parts; radiometer to measure the electromagnetic radiation in the visible, infrared, or microwave spectral bands, imaging radiometer (scanner) to provide a two-dimensional array of pixels from which an image may be produced; and spectroradiometer to measure the radiance in multiple spectral bands (Liang et al., 2012). The Active sensors are emitted electromagnetic radiation to illuminate the observed object. They use a pulse of energy sent by the sensor and receive reflectance of this pulse. The types of measurement tools are included in active sensors are radar which uses a transmitter operating at microwave frequencies to emit electromagnetic radiation, and a directional antenna to measure the time of arrival of reflected pulses from observed objects for determining the distance, synthetic-aperture radar (SAR) which is considered a side-looking radar imaging system that uses the relative motion between an antenna and the Earth surface (Fig. 13.1) to synthesize a very long antenna by combining signals received by the

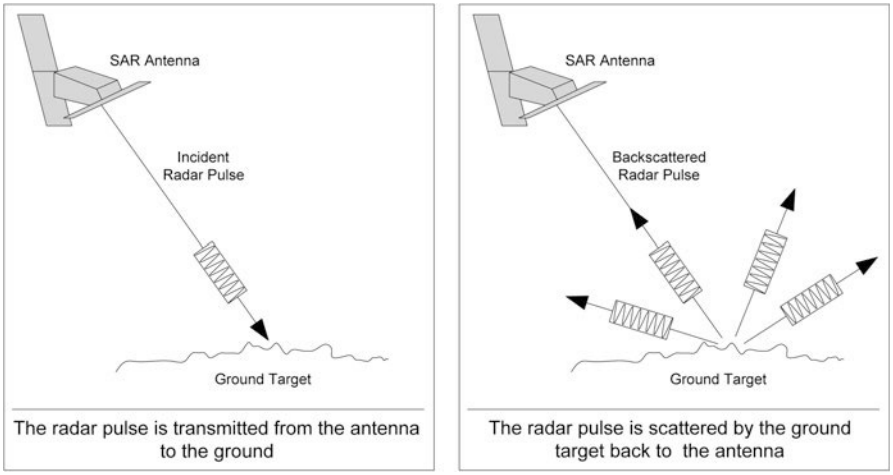

Fig. 13.1 SAR Image production process. https://crisp.nus.edu.sg/~research/tutorial/mw.htm

radar as it moves along its flight track for obtaining high spatial resolution imagery, synthetic interferometric aperture radar (InSAR) which compares two or more amplitude and phase images over the same area received during different passes of the SAR platform at different times, scatterometer which is a high-frequency microwave radar designed specifically to determine the normalized radar cross-section of the surface. LIDAR (Light Detection and Ranging) is an active optical sensor that uses a laser in the ultraviolet, visible, or near-infrared spectrum to transmit a light pulse and a receiver with sensitive detectors to measure the backscattered or reflected light, Laser Altimeter which is a laser altimeter that uses lidar to measure the height of the instrument platform above the surface (Liang et al., 2012).

The specifications of the platform and sensors determine the characteristics of the produced data, including spatial, spectral, temporal, and radiometric resolutions. Spatial resolution refers to the number of pixels representing the construction units of a digital image (Athanasiou et al., 2017). The spatial resolution could identify by the smallest object has been resolved by the sensor, which is also the area of the sensor's field of view (Liang et al., 2012). Figure 13.2 illustrates the difference between the lower and higher levels of spatial resolution.

Spectral Resolution, which represents the range of the electromagnetic spectrum, could be observed by the sensor. The spectral resolution is determined by the number and the narrowness of bands. When the number of bands lies between 3 and 10, this could describe as multispectral resolution, where the hyperspectral resolution includes the number of bands that reach the thousands (Jenice Aroma & Raimond, 2015). Figure 13.3 illustrates the different types of spectral resolution.

Temporal resolution refers to the repeat of the imaging cycle, which means the frequency of processing the same areas with the sensor. Orbit pattern and satellite sensor's design determine the frequency characteristics (Liang et al., 2012). Radiometric resolution represents the smallest energy differences that have been observed from the electromagnetic reflectance. It describes the sensor's ability to detect small changes in radiance and depends on how the continuous upwelling radiance signal is converted to discrete, digital image data. For example, The highly sensitive detector

Fig. 13.2 The difference between the lower and higher levels of spatial resolution. https://crisp.nus.edu.sg/~research/tutorial/image.htm

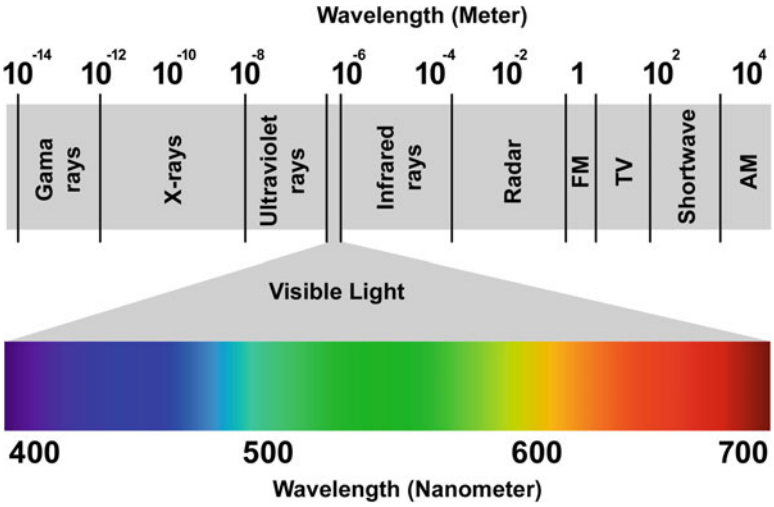

Fig. 13.3 The different types of spectral resolution. https://www.satimagingcorp.com/services/resources/characterization-of-satellite-remote-sensing-systems/

with 12-bit radiometric resolution could be more precise in investigating the water depth of the changing of a channel (Re & Capolongo, n.d.).

13.2.1 Data Types Used in Flood Monitoring

At the MENA region, and due to the lack of data, most flood monitoring research and applications depends on the free available satellite images available remote sensing data. The most widely used satellite images were reviewed from the literature are listed in Table 13.1 (Jenice Aroma & Raimond, 2015).

Depending on the used sensor and techniques, the remote sensing data could be divided into different types. These types are mainly including optical data, multi-spectral data, synthetic aperture radar (SAR) data, and vegetation and water indices. The following section identifies the production process of these types, the uses of each type, and the main differences between them.

13.2.2 Optical Data

Optical imaging depending on the visible, near-infrared, and shortwave infrared spectrums to produce the imagery types such as panchromatic, multispectral, and hyperspectral as shown in Fig. 13.4 (Zhu et al., 2018). Optical data is considered a crucial data source in the investigation of flood extension and evolution. Clean water

Table 13.1 A review for the most used remote sensing data in flood monitoring

Satellite Name	Lunched by	Purpose	Details
Landsat	National Aeronautics and Space Administration (NASA)	Land cover, forest and agricultural applications	The Landsat 7 images are of 30 m spatial resolution for multispectral and 15 m for panchromatic mode (PAN) images
Resourcesat	Indian space research organization (ISRO) offers		Available to the public users with 23.5 m and 56 m resolution, respectively
Terra	Nasa	Collecting information about both the earth surface and atmosphere	- advanced Spaceborne thermal emission and reflection Radiometer (ASTER) - clouds and Earth's radiant energy system (CERES) Multi-angle imaging Spectroradiometer (MISR), moderate resolution imaging Spectroradiometer (MODIS) - measurements of pollution in the troposphere (MOPITT).
Aqua	Nasa	Collecting information about the earth's water cycle, glaciers, and atmosphere	
Calipso	Nasa	Atmospheric, aerosol activity, and effective climate research	The Lidar instrument combined with passive infrared and visible imagers could capture the cloud movement and aerosol properties [
Earth Observing-1	Nasa		Hyperspectral imager could measure up to 200 wavelengths
Quickbird	Digital globe		Very high-resolution satellite images of 60 cm in PAN and 2.4 m in multispectral images
Formosat	National Space Organization (NSPO) of the republic of China.		High-resolution images of 2 m in PAN and 8 m in multispectral images
Spot	French organization named spot image		Offer 2.5 m to 5 m in PAN and 10 m in multispectral. Mode
Ikonos	GeoEye organization [20].		Providing high resolution multispectral and PAN images of 4 m and 1 m, respectively
Sentinel	European Space Agency (ESA)	Land cover change analysis and natural disasters monitoring applications	Provides all-weather data both day and night on radar imaging

(continued)

Table 13.1 (continued)

Satellite Name	Lunched by	Purpose	Details
Kalpana			Produces three bands of visible, thermal infrared, and water vapor infra-red images using a very high-resolution radiometer (VHRR) with a resolution of 2 × 2 km [22].
Radarsat	Canadian Space Agency (CSA)	Landcover operations on mines, icebergs, and underground water explorations	Offers SAR data which

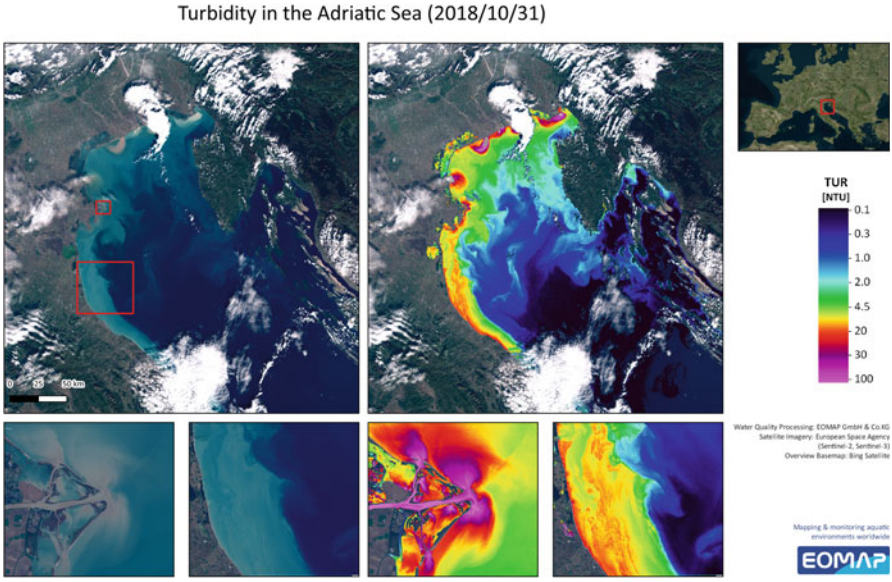

Fig. 13.4 "Left images, captured on October 31, 2018, show the large river sediment inflows into the Northern Adriatic Sea in "true" color. The right images display the turbidity levels assessed with EOMAP's EO processing system" (https://www.eomap.com/using-satellite-data-for-flood-monitoring/)

surfaces absorb most of the electromagnetic energy. Therefore, in optical images, the water area could be recognized easily where it appears as dark areas. However, in cases such less clean water and increasing reflections from water recognition is becoming more difficult, and using several spectral bands data can help (Fig. 13.5). Cloud coverage is the main obstacle that faces the use of optical data in flood monitoring, which are often associated with flood events (Re & Capolongo, n.d.).

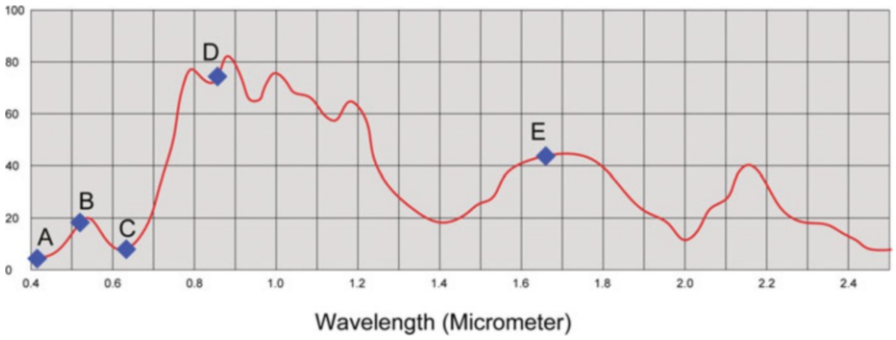

Fig. 13.5 Typical Reflectance Spectrum of Vegetation. The labeled arrows indicate the common wavelength bands used in optical remote sensing of vegetation: (**a**): blue band, (**b**): green band; (**c**): red band; (**d**): near IR band; (**e**): short-wave IR band (https://crisp.nus.edu.sg/~research/tutorial/optical.htm)

13.2.2.1 Multispectral Data

Multispectral remote sensing data is produced by a multispectral sensor. The used sensors have multichannel detectors; each channel is sensitive to radiation within a narrow wavelength band. These sensors produce multilayer image which contains both the brightness and spectral information for the objects. A hyperspectral sensor collects and processes information from 10 to 100 spectral bands. The resulting images can be used in recognizing objects, identify materials, and detect elemental components (Zhu et al., 2018). A multispectral sensor could be useful in flood monitoring with a presence of cloud coverage and within dense urban areas (Vissers, 2007).

13.2.2.2 Synthetic Aperture Radar (SAR) Data

Synthetic aperture radar (SAR) is useful in mapping the object's reflectivity with high spatial resolution through the emission and reception of electromagnetic pulses. The SAR data have various applications such as detecting objects and their geographic location, estimation of environments geophysical properties (i.e. certain dimensions, moisture content, roughness, and density) (Ditchfield, 1966).

Synthetic aperture radar data are a valuable resource for monitoring flood events. Most of the flood events have been accompanied by the widespread presence of clouds; the long-wavelength in SAR system could propagate through these clouds, which provied accurate data images.SAR sensors have achieved unprecedented resolutions and repetitivity of acquisition so that their application to flood monitoring is receiving mounting interest (Re & Capolongo, n.d.).

13.2.2.3 Vegetation and Water Indices

The spectral composition of remote sensing spectral data provides information about the physical properties of soil, water, and vegetation features in terrestrial environments. Remote sensing techniques, models, and indices are designed to convert this spectral information into a form that is easy to interpret (Bannari et al., 2017). Indices are considered a compact form of data that can effectively ensure the presence or absence of water. The indices are common identified as quantitative comparisons between the response of each ground pixel in different bands of the electromagnetic spectrum (Re & Capolongo, n.d.).

Several indices have been developed, such as the Normalized Difference Water Index (NDWI), proposed by McFeeters in 1996 to detect surface waters in wetland environments and investigate the surface water extent(Mcfeeters, 2013). Also, the Normalized Difference Vegetation Index (NDVI) is applied to estimate the level of crop's growth and detect the drought rate of vegetation (Mcfeeters, 2013). On the other hand, water emission in the infrared is generally lower than in the red part of the spectrum, so water has an inverse NDVI behavior with respect to both vegetated and unvegetated land. This makes NDVI a suitable tool to detect water surfaces rapidly (Re & Capolongo, n.d.).

13.3 Potential and Limitations of Open Satellite Data for Flood Mapping

13.3.1 Cloud Coverage Problem

In spite of the great potential that remote sensing in flood management, some limitations face its use. For example, the presence of cloud cover during the flood event has been reported as the major challenge in the use of optical remote sensing in flood management. According to Sanyal and Lu (2004), using SAR is a better option because of the higher penetration power of the radar pulse, overcoming the problem. However, its use, especially in developing countries has been constrained by its high prices as well as limited coverage (Application of Remote Sensing and Geographical Information Systems in Flood Management: A Review). Figure 13.6 provide an example of the cloud coverage effect on the remote sensing data.

Furthermore, spatial resolution has a crucial effect on flood monitoring. The spatial characteristics of the flood inundation area could constrain the use of satellite images with lower spatial resolution. When the inundated area is small, it cannot be observed by low-resolution images. Also, urban areas or dense forests complicate the process of flood detection. However, the high-resolution data and field surveys are crucial for reliable mapping (Potential and limitations of open satellite data for flood mapping).

Fig. 13.6 The Sentinel-2 cloudless layer combines over 80 trillion pixels collected during differing weather conditions between May 2016 and April 2017. Image: ESA. (https://medium.com/planet-stories/cloudless-an-open-source-computer-vision-tool-for-satellite-imagery-6f4daaa4851f)

13.3.2 The Problem of Temporal Resolution in Flood Management

Temporal resolution represents a further challenge that faces the use of remote sensing in flood monitoring. The low temporal resolution causes limited availability of imageries in time-space, seasonal variations, and different technical limitations. For example, low temporal resolution may cause to not capture the peak of the flood event where most radar images are taken sometime before it. In addition, an area flooded by a small stream has a very short co-flood time interval which necessitates the higher temporal resolution. There is an essential need for a more consistent monitoring strategy in terms of frequency and timeliness of remote sensing data collection. The inadequate frequency of image collection is one of the most important limitations. It is found that the closer the time between when the image data were collected and when the event peak occurred, the more reliable the detection of maximum flood extents and depths.

13.3.3 The Problem of Detecting Flooding in Urban Areas

Floodwaters can be detected with good precision by exploiting several typical characteristics of inland water surfaces with respect to dry areas. One is the reduced reflectance of clean and calm water with respect to land areas. This behavior is common to virtually all the optical spectral ranges, as long as the acquisition is far from the specular direction. An additional way to distinguish the presence of surface water is given by the availability of reflectance information in the infrared thermal spectral bands. This is also generally low for water surfaces with respect to land areas. Both these methods rely on assumptions that are broadly fulfilled when monitoring flood events occurring over non-urban land areas, especially when using low or medium-resolution data. For instance, artificial surfaces may have very low reflectance and thus be mistaken for flooded areas. This is more likely to occur in highly complex environments like urban areas, where pavements and tarmacs may have a wide range of reflectance behaviors during a flood event. This may also include flooded surfaces exhibiting artificially high reflectance, which could be due, for instance, to a shallow water layer over a bright pavement or to specular reflections from surrounding buildings. Such cases could be successfully solved by sensors having infrared detection bands. In fact, urban areas are admittedly among the most complicated land cover types for many remote sensing applications, in virtually all regions of the electromagnetic spectrum, with flood monitoring making no exception (Re & Capolongo, n.d.).

13.4 Application of Remote Sensing on Flash Flood and Extreme Rainfall Events in MENA Region

13.4.1 Area of Interest

The surface area of the Arab region is about 13,781,751 km^2. It consists of 22 countries as shown in the map (Fig. 13.8a). The population has increased by the rate of 2% every year from 2002 to 2020. The average annual rainfall over the Arabian region varies from 0 to 1800 mm, while the average evaporation rate is more than 2000 mm/year (https://data.worldbank.org/indicator/SP.POP.GROW?view=map (2021); Saber et al., 2017b). The Arab region is suited in the northern hemisphere with semi-arid to arid climatic conditions. The total average rainfall (Fig. 13.7a) estimated from GSMaP shows spatial variability with a low precipitation rate over the region (Saber et al., 2017a). The aridity index was estimated for the region from The Consortium for Spatial Information (CGIAR-CSI) [8)] as shown in (Fig. 13.7b). In most Arabian countries, during the last 7 years, Wadi flash floods (WFF) became catastrophic and more frequent in both space and time (Fig. 13.8a & b).

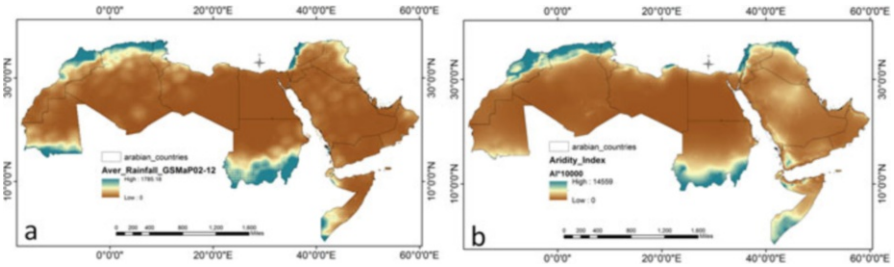

Fig. 13.7 Average rainfall estimated from Global Satellite Mapping of Precipitation (GSMaP) data (**a**) and Aridity Index (**b**) estimated from Global Aridity Index developed by the Consortium for Spatial Information (CGIAR-CSI) 2002–2012

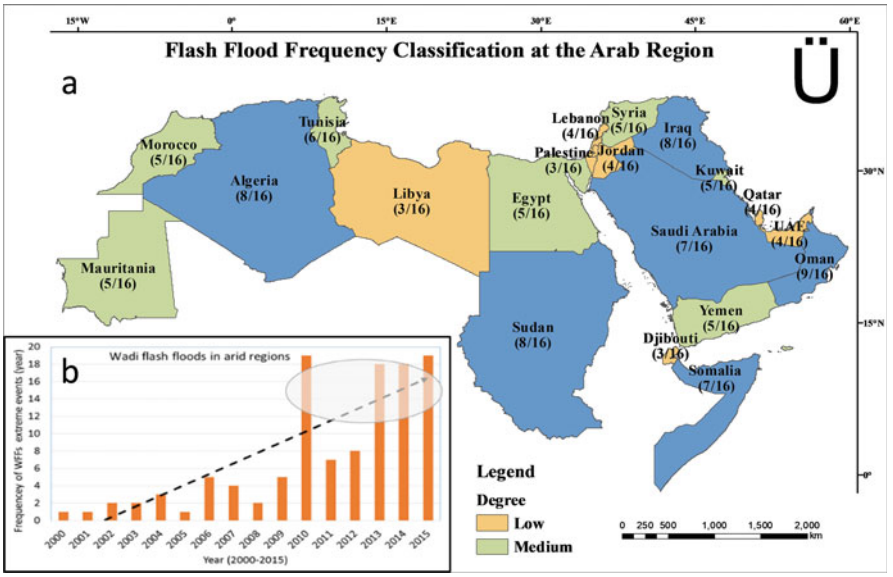

Fig. 13.8 Wadi flash floods frequency and classification spatially (**a**) and temporally (**b**) at the Arab region

13.4.2 Case Study of Cities of (Al Arish, Ras Gharib, Al Saloum, Drunka, Hurghada)

According to the UNDP, by 2050, two-thirds of the world's population is likely to live in cities. Urban flooding is already a major risk for cities. Increasing impervious surface area, inadequate stormwater drainage, and aging infrastructure all contribute. As a result, growing urban populations will face a greater risk of flooding from extreme weather events. Using satellite data allows individuals and organizations to develop better plans for handling floods. This can include developing better early

warning techniques, better plans for rescue and relief, and more effective long-term infrastructure planning.

In Egypt, about half of the yearly precipitation falls from December to March. Precipitation is generally very low throughout the country, although it averages more than 200 mm/year along the Mediterranean coastline. Most of Egypt is a desert and is classified as arid, except for the Mediterranean coast, semi-arid. There are four climate regions in Egypt: Nile Valley (from Cairo to Assiut, from Assiut to Edfu and from Edfu to Nasser Lake), Eastern Desert (Red Sea Region), Sinai Peninsula (South Sinai and North Sinai), and Matrouh Governorate (Salloum Plateau). Our goal is to generalize the results for the whole country. Therefore, representative samples with different climatic regions in Egypt and the selection of case studies were conducted based on two factors: the history of hazardous flash floods and climatic conditions. Accordingly, the selected cities are the city of "Ras Gharib" representing the Red Sea and Eastern Desert region, the city of "Al-Arish" representing the region of the Sinai Peninsula, "Drunka village" in Assiut governorate representing the Nile Valley and Delta region, and the city of "Salloum" that is representative of the Mediterranean region (Saber et al., 2020).

Ras Gharib is the second-largest city in Red Sea Governorate and the most important Egyptian city in oil production. It is located 150 km to the north of Hurghada on the Red Sea coast (Fig. 13.4d). Ras Gharib is considered to have a desert climate. During the year, there is virtually no rainfall, with an average of about 5 mm. The average annual temperature is about 22.2 °C (Saber et al., 2020).

The Sinai Peninsula is located in the northeast of Egypt between latitudes 27°43′ to 29°55′ and longitude 32°39′ to 34°52′. Al-Arish (Fig. 13.4b) is located on the coast of the Mediterranean Sea. It has a tropical climate with a rainfall average of about 3262 mm, even during the driest months. The average annual temperature is 23.8 °C (Saber et al., 2020).

Salloum is a small Egyptian border city near the western border of Egypt with Libya. It is located on the Mediterranean coast (Fig. 13.4d). The climate in Salloum is considered a desert climate. The average annual temperature is 19.6 °C, and the average annual rainfall is 150 mm (Saber et al., 2020).

Drunka is one of the villages of Asyut Center in Asyut Governorate in Egypt (Fig. 13.4c). The climate in Asyut is called a desert climate, with a precipitation average of about 2 mm, and the average annual temperature is 22.6 °C (Saber et al., 2020).

Hurghada is an essential center for tourist and mining activities: it lies directly on the Red Sea coast, and it is bounded by latitudes 270° 10′ and 270° 30' N and longitudes 330° 30′ and 330° 52′ E. Hurghada almost every year, causing loss of life and significant damage. Accordingly, the city has become one of the most vulnerable areas to such events near the Red Sea. Satellite rainfall data show that this trend increased in Hurghada from 1983 to 2019. Additionally, the city has the highest mean annual maximum daily precipitation in Egypt. Since 2000, numerous urban flash flood events have occurred along the Egyptian Red Sea coast, which has experienced 30 medium and large events this century (Gado, 2017). There has

been an increase in the exposure of the city to flood risk during winter (rainy season) from October to February due to convective rainfall (Table 13.1).

Additionally, since 1996, several urban flash flood events have been recorded in the city and its vicinity. Inhabited areas, main roads, military campuses, and tourist buildings have been severely affected. Moreover, environmental contamination due to water flooding, especially in the inhabited lowland areas, has occurred (Abdrabo et al., 2020a) (Fig. 13.9).

13.4.3 Remote Sensing Data

Many types of data sets were collected and analyzed in this study (Table 13.2 and Fig. 13.10). The lack of hydrological and meteorological data in the Egyptian cities necessitated the use of hydrological modeling to predict flood depth and the spatial extent and identify sites with high risk. The RRI model used several remote-sensing data, including a digital elevation model (DEM) with an accuracy of 12.5 m, an LC map, and historical daily rainfall records. The resolution of the rainfall data was as follows: (0.04° × 0.04°)-hourly based data for the 2014 (5-year REP) and 2016 (10-year REP) events. The resolution of the rainfall data was (0.25° × 0.25°)-daily based data on the 1996 (50-year REP) event. LC was mapped from Sentinel (2A) with a 30 m resolution. These data sets were used to produce the inundation maps for the 5, 10, and 50 REPs in Hurghada.

Regarding model calibration and validation, photos during the event from different local newspapers were used. One of the authors (S.A.K.) conducted fact-finding and field investigations, reconnaissance-level inventories for topographic maps, and site visits to obtain the ground truth of the interpretations from imagery. From 2014 to 2015, we visited several specific urban sites, reviewed the proposed layouts of buildings and infrastructure, and provided comments to developers regarding avoiding urban flash flood risk and other environmental impacts. We have direct knowledge of the urban flash flood history of Hurghada over the past three decades, from the early 1980s to 2019.

13.4.4 Methodology

The workflow of the hazard module for floods using the RRI model is summarized in three steps. First, the daily spatial rainfall intensities for different hazard scenarios were obtained based on PERSIANN-Climate Data Record (CDR) for the 1996 event and the PERSIANN-Cloud Classification System (CCS) for the 2014 and 2016 events with their highest resolutions, i.e., 25 km and 4 km, respectively. Second, the DEM was obtained from Advanced Land Observation System-Phased Array Synthetic Aperture Radar (ALOS-PALSAR) data available from the Alaska Satellite Facility (ASF) Distributed Active Archive Center (DAAC) with a 12.5 m resolution

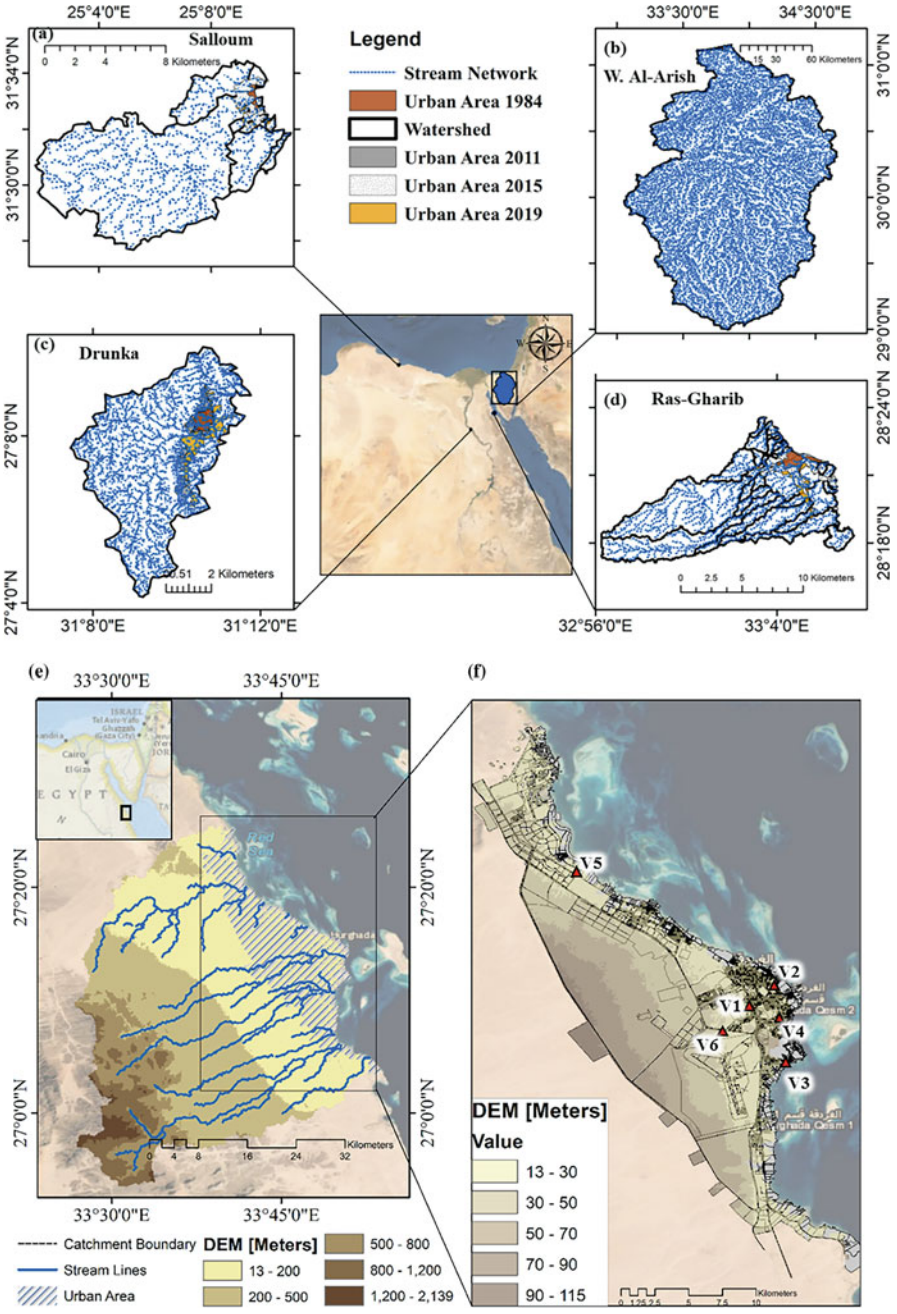

Fig. 13.9 Location maps showing the target cities and related wadi catchments and stream network developed from DEM (Sentinel-2) by GIS: (**a**) Salloum, (**b**) Wadi Al-Arish, (**c**) Drunka, (**d**) Ras Gharib, (**e**) the Hurghada catchment area, and (**f**) Hurghada city

Table 13.2 Material descriptions

Data type	Date	Format	Data source	Derived data
ASTER-ALSO-PALSAR (12.5 m spatial resolution)	2020	Geotiff	[84]	Topographic and hydrological parameters
Rainfall (scale 0.04° × 0.04°) (hourly based)	2020	PERSIANN-CCS	[85]	Rainfall distribution during the 2014 and 2016 events
Rainfall (scale 0.25° × 0.25°) (daily based)		PERSIANN-CDR	[86]	Rainfall distribution during the 1994 event
Sentinel (2A) (30 m resolution)	2019	Geotiff	[87]	Land cover types

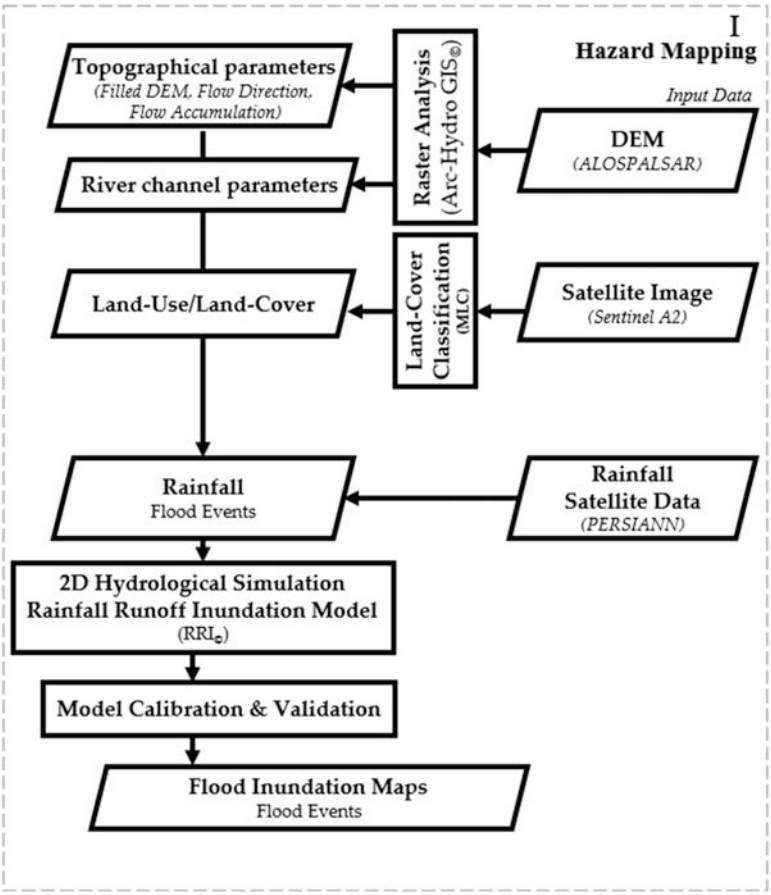

Fig. 13.10 Flowchart for data processing and methods

(ASF, 2006). The original DEM was processed using the Arc-hydro tool of ArcMap 10.6.1 to obtain the filled DEM, and the flow direction and flow accumulation were extracted. The Arc-hydro tool was used later to identify and extract the drainage

features in the study areas, such as the flow direction, flow accumulation, stream networks, and watershed delineation required as inputs for the RRI model. Third, the LC map was created based on the Sentinel-2A satellite data from 2019, which were corrected based on Google Earth satellite images (General Organization for Physical Planning (GOPP), 2013, 2018). The initial parameters of the RRI model were assigned based on the validated parameters in arid regions (Abdel-Fattah et al., 2016). Finally, the RRI input raster maps for rainfall, topography, and LC were converted into ASCII files with their original resolutions, while the hazard maps (inundation depths) had the same resolution as the DEM utilized (12.5 m × 12.5 m).

- Model calibration and validation

For more comprehensive and accurate results, the RRI model was calibrated and validated. Due to the lack of observed data, the calibration and validation processes were performed based on reported images of the simulated events in each city. Regarding the land use parameters in the RRI model, the city was classified into three types of land use: desert, vegetation, and urban, in order to determine the model parameters for different cases.

13.4.5 Results and Discussions

In the case mentioned above studies, remote sensing data were used as input to distributed hydrological models to predict streamflow at the microscale scale catchments better. The results as shown in Figs. 13.6 and 13.7, which is already described in (Abdrabo et al., 2020b; Saber et al., 2020), showed encouraging results using global datasets combined with in-situ data. Moreover, it showed that model results using the remote sensing products combined with in-situ data were generally accurate (Figs. 13.11, 13.12 and 13.13).

13.5 Conclusion

In this chapter, a summary of the most important aspects of detailed flood monitoring through remote sensing has been attempted. We reviewed the basics of flood monitoring practices, focusing on the commonly accepted standards for definition, detection, and updating of flood maps. We then listed the primary sources of data that are commonly used in flood monitoring activities, spanning through optical and microwave instruments, the main sources of remotely sensed data used in this field.

The importance of using satellite-based products was discussed for application in arid regions where the data are not available. We focused mainly on the general idea of the main data processing techniques used to extract flood inundation maps and evolution information from earth observation data and to integrate remotely sensed data into hydrological inundation models, as well as to use remote sensing-derived

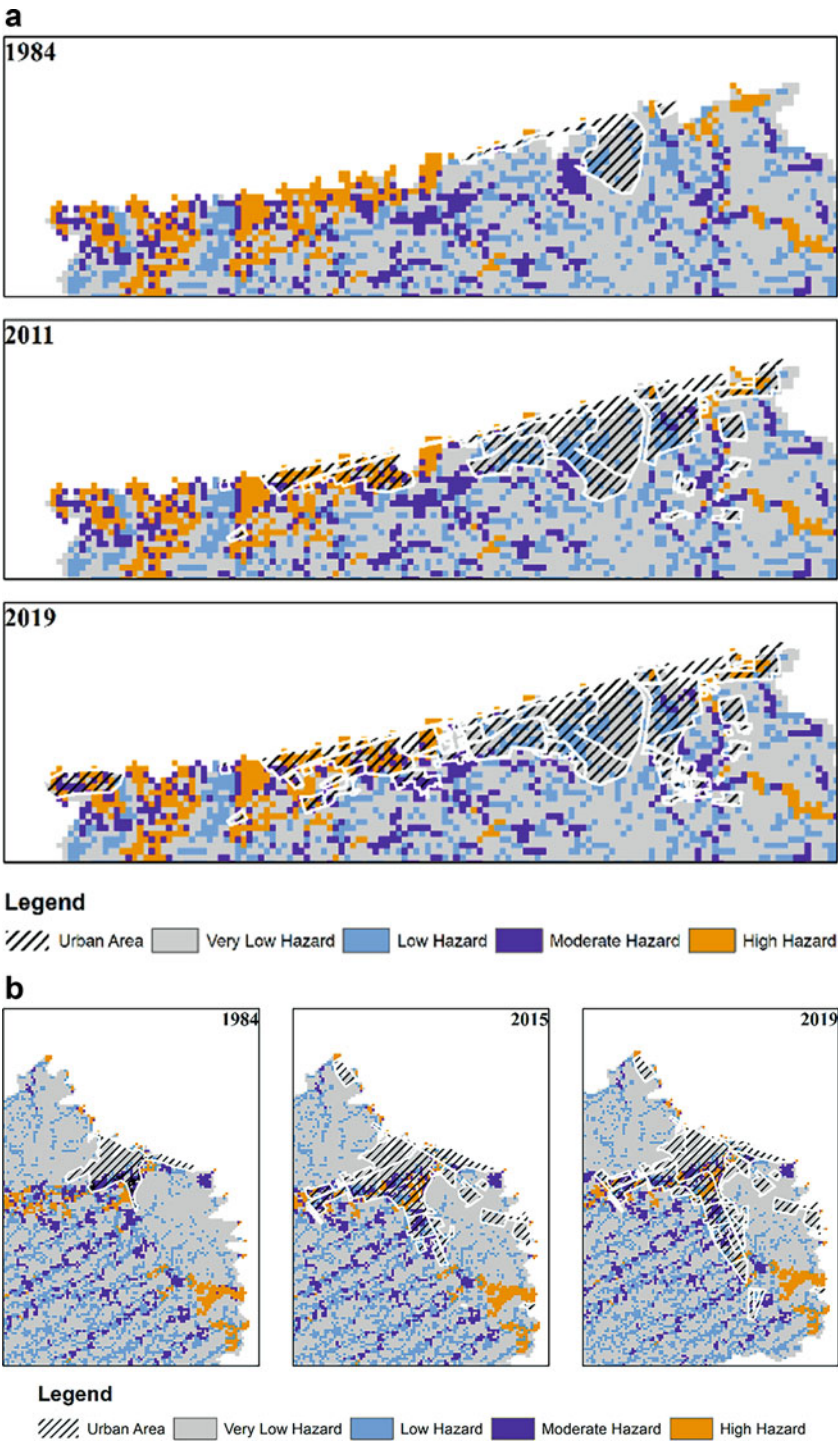

Fig. 13.11 Inundation maps showing the hazard levels affecting the urban areas (**a**) and estimates of the vulnerable areas for flood hazard categories from1984-2019 in (**a**) Al-Arish, (**b**) Ras Gharib, (**c**) Salloum, and (**d**) Drunka

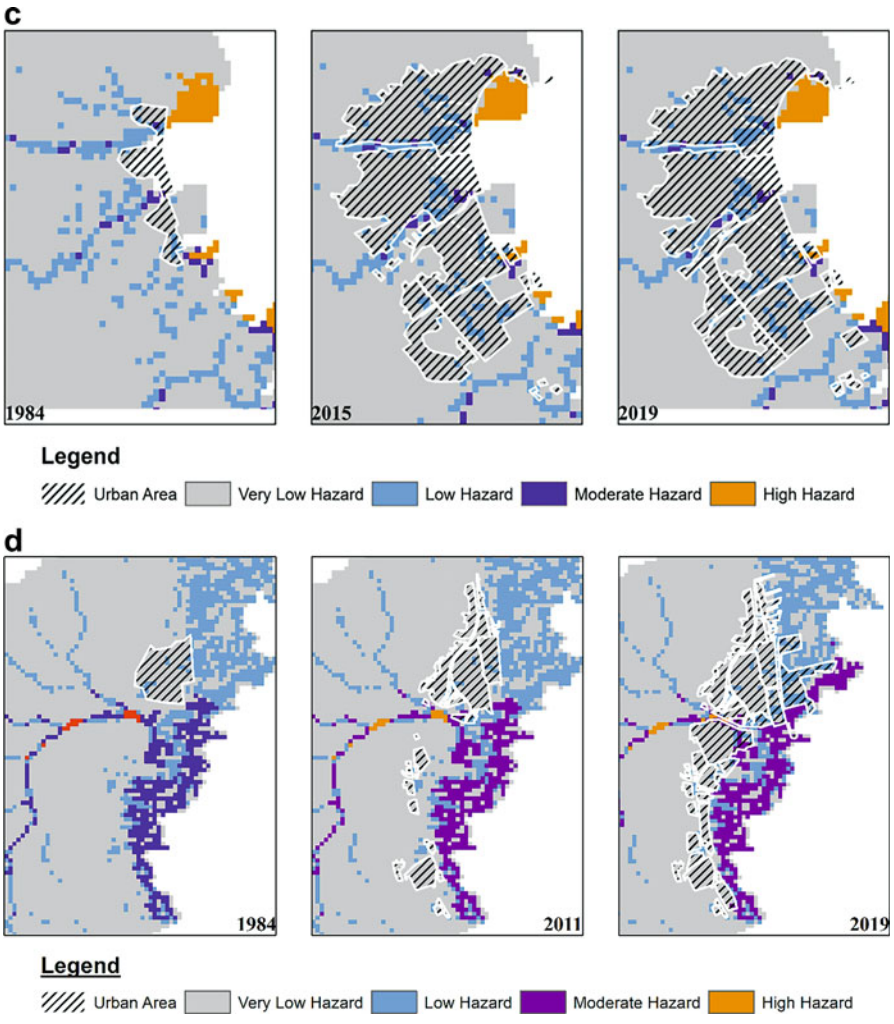

Fig. 13.11 (continued)

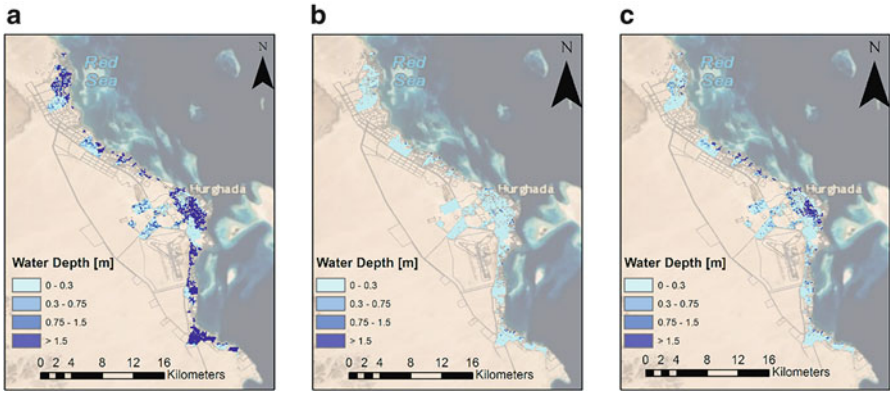

Fig. 13.12 Flood inundation maps (RRI model) for Hurghada in 1996, 2014 and 2016 (**a**–**c**)

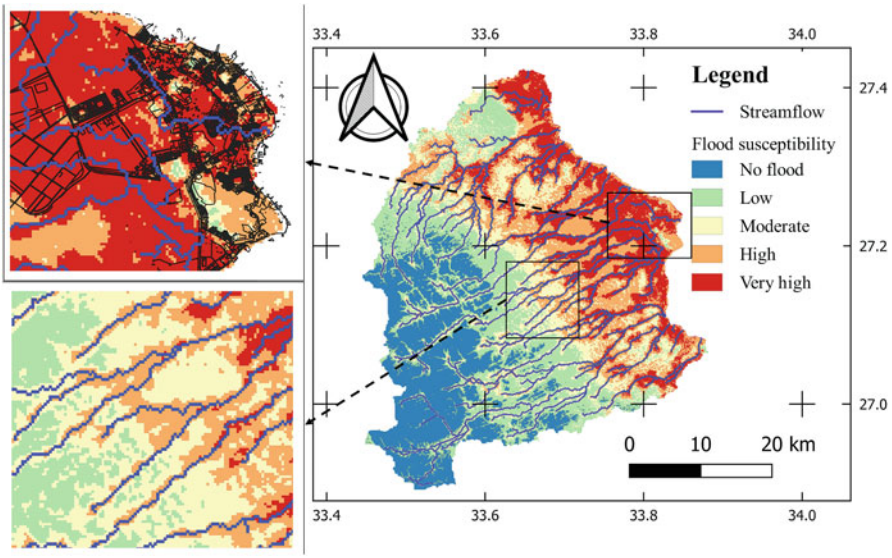

Fig. 13.13 Hurghada Flood susceptibility maps based on the Machine learning method (LightGBM) in 2021. (Source: Saber et al., 2021)

information to enrich our knowledge of flood processes and aid decision-making systems.

References

(ASF), Alaska Satellite Facility. (2006). *DEM 30 m*. Retrieved March 12, 2020 (https://search.asf.alaska.edu/#/?dataset=ALOS&zoom=7.334585016709559¢er=28.682014,29.484976&polygon=POINT(29.7851%2031.1334)&resultsLoaded=true&granule=ALPSRP141900610-KMZ).

Abdel-Fattah, M., Kantoush, S. A., Saber, M., & Sumi, T. (2016). *Hydrological modelling of flash flood in Wadi Samail, Oman*. Kyoto university.

Abdrabo, K. I., Kantoush, S. A., Saber, M., Sumi, T., Habiba, O. M., Elleithy, D., & Elboshy, B. (2020a). Integrated methodology for urban flood risk mapping at the microscale in ungauged regions: A case study of Hurghada, Egypt. *Remote Sensing, 12*(21), 3548. https://doi.org/10.3390/rs12213548

Abdrabo, K. I., Kantoush, S. A., Saber, M., Sumi, T., Habiba, O. M., Elleithy, D., & Elboshy, B. (2020b). Integrated methodology for urban flood risk mapping at the microscale in ungauged regions: A case study of Hurghada, Egypt. *Remote Sensing, 12*(21), 3548. https://doi.org/10.3390/rs12213548

Abushandi, E. H., & Merkel, B. J. (2011). Application of IHACRES rainfall-runoff model to the Wadi Dhuliel arid catchment, Jordan. *Journal of Water and Climate Change, 2*(1), 56–71.

Ali, S. A., Khatun, R., Ahmad, A., & Ahmad, S. N. (2019). Application of GIS-based analytic hierarchy process and frequency ratio model to flood vulnerable mapping and risk area estimation at Sundarban region, India. *Modeling Earth Systems and Environment, 5*(3), 1083–1102.

Ali, S. A., Parvin, F., Pham, Q. B., Vojtek, M., Vojteková, J., Costache, R., Linh, N. T. T., Nguyen, H. Q., Ahmad, A., & Ghorbani, M. A. (2020). GIS-based comparative assessment of flood susceptibility mapping using hybrid multi-criteria decision-making approach, Naïve Bayes tree, bivariate statistics and logistic regression: A case of Topľa Basin, Slovakia. *Ecological Indicators, 117*, 106620.

Arora, A., Arabameri, A., Pandey, M., Siddiqui, M. A., Shukla, U. K., Bui, D. T., Mishra, V. N., & Bhardwaj, A. (2020). Optimization of state-of-the-art fuzzy-metaheuristic ANFIS-based machine learning models for flood susceptibility prediction mapping in the middle ganga plain, India. *Science of the Total Environment, 750*, 141565. https://doi.org/10.1016/j.scitotenv.2020.141565

Athanasiou, L. S., Fotiadis, D. I., & Michalis, L. K. (2017). Propagation of segmentation and imaging system errors. *Atherosclerotic Plaque Characterization Methods Based on Coronary Imaging, 151–66*. https://doi.org/10.1016/b978-0-12-804734-7.00008-7

Bannari, A., Morin, D., Bonn, F. & Huete, A. R.. 2017. *A review of vegetation indices*. 7257(April). https://doi.org/10.1080/02757259509532298.

Bisht, S., Chaudhry, S., Sharma, S., & Soni, S. (2018). Assessment of flash flood vulnerability zonation through geospatial technique in high altitude Himalayan watershed, Himachal Pradesh India. *Remote Sensing Applications: Society and Environment, 12*, 35–47.

Chen, S., Junjun, H., Zhang, Z., Behrangi, A., Hong, Y., Gebregiorgis, A. S., Cao, J., Baoqing, H., Xue, X., & Zhang, X. (2015). Hydrologic evaluation of the TRMM multisatellite precipitation analysis over Ganjiang Basin in humid Southeastern China. *IEEE Journal of Selected Topics in Applied Earth Observations and Remote Sensing, 8*(9), 4568–4580.

Ditchfield, C. R. (1966). Microwave radiometry. *Journal of Navigation, 19*(4), 503–521. https://doi.org/10.1017/S0373463300047639

Domeneghetti, A., Schumann, G. J. P., & Tarpanelli, A. (2019). Preface: Remote sensing for flood mapping and monitoring of flood dynamics. *Remote Sensing, 11*(8), 943. https://doi.org/10.3390/rs11080943

Gado, T. A. (2017). *Statistical characteristics of extreme rainfall events in Egypt* (pp. 18–20).

General Organization for Physical Planning (GOPP). (2018). *General strategic plan of 2027 for proposed future urbanization area for the city of Tanta*.

General Organization for Physical Planning (GOPP), Ministry of Housing. (2013). *General strategic plan of 2027 for proposed future urbanization area for the city of Hurghada, Red Sea*. Cairo, Egypt.

Hall, J., Arheimer, B., Borga, M., Brázdil, R., Claps, P., Andrea Kiss, T. R., Kjeldsen, J. K., Kundzewicz, Z. W., & Lang, M. (2014). Understanding flood regime changes in Europe: A state-of-the-art assessment. *Hydrology and Earth System Sciences, 18*(7), 2735–2772.

Haq, M., Akhtar, M., Muhammad, S., Paras, S., & Rahmatullah, J. (2012). Techniques of remote sensing and GIS for flood monitoring and damage assessment: A case study of Sindh Province, Pakistan. *The Egyptian Journal of Remote Sensing and Space Science, 15*(2), 135–141. https://doi.org/10.1016/j.ejrs.2012.07.002

Hsu, K.-l., Gao, X., Sorooshian, S., & Gupta, H. V. (1997). Precipitation estimation from remotely sensed information using artificial neural networks. *Journal of Applied Meteorology, 36*(9), 1176–1190.

Hutter, G. (2006). Strategies for flood risk management–A process perspective. In *Flood risk management: Hazards, vulnerability and mitigation measures* (pp. 229–246). Springer.

Jenice Aroma, R., & Raimond, K. (2015). A review on availability of remote sensing data. In *Proceedings – 2015 IEEE international conference on technological innovations in ICT for agriculture and rural development, TIAR 2015* (pp. 150–155). TIAR. https://doi.org/10.1109/TIAR.2015.7358548

Joyce, R. J., Janowiak, J. E., Arkin, P. A., & Xie, P. (2004). CMORPH: A method that produces global precipitation estimates from passive microwave and infrared data at high spatial and temporal resolution. *Journal of Hydrometeorology, 5*(3), 487–503.

Kilpatrick, F. A., & Cobb, E. D. (1985). *Measurement of discharge using tracers*. Department of the Interior, US Geological Survey.

Kneis, D., Chatterjee, C., & Singh, R. (2014). Evaluation of TRMM rainfall estimates over a large Indian River Basin (Mahanadi). *Hydrology and Earth System Sciences, 18*(7), 2493–2502.

Kummerow, C., Barnes, W., Kozu, T., Shiue, J., & Simpson, J. (1998). The tropical rainfall measuring mission (TRMM) sensor package. *Journal of Atmospheric and Oceanic Technology, 15*(3), 809–817.

Liang, S., Li, X., & Wang, J. (2012). *A systematic view of remote sensing*.

Lin, X. (1999). Flash floods in arid and semi-arid zones. *Technical Documents in Hydrology*.

Martín-Vide, J. P., & Llasat, M. C. (2018). The 1962 flash flood in the Rubí stream (Barcelona, Spain). *Journal of Hydrology, 566*, 441–454.

Mcfeeters, S. K. (2013). *Using the normalized difference water index (NDWI) within a geographic information system to detect swimming pools for mosquito abatement: A practical approach* (pp. 3544–3561). https://doi.org/10.3390/rs5073544

Ochoa, A., Pineda, L., Crespo, P., & Willems, P. (2014). Evaluation of TRMM 3B42 precipitation estimates and WRF retrospective precipitation simulation over the Pacific–Andean region of Ecuador and Peru. *Hydrology and Earth System Sciences, 18*(8), 3179–3193.

Ozturk, U., Wendi, D., Crisologo, I., Riemer, A., Agarwal, A., Vogel, K., López-Tarazón, J. A., & Korup, O. (2018). Rare flash floods and debris flows in Southern Germany. *Science of the Total Environment, 626*, 941–952.

Pilgrim, D. H., Chapman, T. G., & Doran, D. G. (1988). Problems of rainfall-runoff modelling in arid and semiarid regions. *Hydrological Sciences Journal, 33*(4), 379–400.

Prasetia, R., As-syakur, A. R., & Osawa, T. (2013). Validation of TRMM precipitation radar satellite data over Indonesian region. *Theoretical and Applied Climatology, 112*(3), 575–587.

Re, A., & Capolongo, A. D. (n.d.) *Monitoring through remote sensing.*

Refice, A., D'Addabbo, A., & Capolongo, D. (Eds.). (2018a). *Flood monitoring through remote sensing*. Springer.

Refice, A., D'Addabbo, A., & Capolongo, D. (2018b). Methods, techniques and sensors for precision flood monitoring through remote sensing. In *Flood monitoring through remote sensing* (pp. 1–25). Springer.

Rodier, J., & Roche, M. (1978). River flow in arid regions. *Hydrometry: Principles and Practices, 453*.

Saber, M., & Habib, E. (2016). Flash floods modelling for Wadi System: Challenges and trends. In *Landscape dynamics, soils and hydrological processes in varied climates* (pp. 317–339). Springer.

Saber, M., Hamaguchi, T., Kojiri, T., & Tanaka, K. (2010). *Flash flooding simulation using hydrological modeling of Wadi Basins at Nile River Based on satellite remote sensing data* 16.

Saber, M., Kantoush, S. A., & Sumi, T. (2017a). *Assessment of water storage variability using grace and gldas data in the Arabian countries considering implications for water resources management* (pp. 13–18).

Saber, M., Alhinai, S., Al Barwani, A., Ahmed, A. L.-S., Kantoush, S. A., Habib, E., & Borrok, D. M. (2017b). Satellite-based estimates of groundwater storage changes at the Najd Aquifers in Oman. In *Water resources in arid areas: The way forward* (pp. 155–169). Springer. https://data.worldbank.org/indicator/SP.POP.GROW?view=map (2021)

Saber, M., Abdrabo, K. I., Habiba, O. M., Kantosh, S. A., & Sumi, T. (2020). Impacts of triple factors on flash flood vulnerability in Egypt: Urban growth, extreme climate, and mismanagement. *Geosciences, 10*(1), 24.

Saber, M., Boulmaiz, T., Guermoui, M., Abdrado, K. I., Kantoush, S. A., Sumi, T., Boutaghane, H., Nohara, D., & Mabrouk, E. (2021). Examining LightGBM and CatBoost models for Wadi flash flood susceptibility prediction. *Geocarto International*, 1–26.

Sanyal, J., & Lu, X. X. (2004). Application of remote sensing in flood management with special reference to Monsoon Asia: A review. *Natural Hazards, 33*(2), 283–301.

UNISDR, C. 2015. The human cost of natural disasters: A global perspective.

University of Waterloo, Nick Kouwen, Eric Soulis, and University of Waterloo. (1993). Remote sensing inputs for flash flood forecasting in urban areas. *Journal of Water Management Modeling*. https://doi.org/10.14796/JWMM.R175-08

Vissers, M. (2007). K & C Science Report – Phase 1 Tropical Forest and Wetlands Mapping , Case Study Borneo. (January).

Wheater, H., Sorooshian, S., & Sharma, K. D. (2007). *Hydrological modelling in arid and semi-arid areas*. Cambridge University Press.

Yoshimoto, S., & Amarnath, G. (2017). Applications of satellite-based rainfall estimates in flood inundation modeling—A case study in Mundeni Aru River basin, Sri Lanka. *Remote Sensing, 9*(10), 998.

Zhang, X., Aguilar, E., Sensoy, S., Melkonyan, H., Tagiyeva, U., Ahmed, N., Kutaladze, N., Rahimzadeh, F., Taghipour, A., & Hantosh, T. H. (2005). Trends in Middle East climate extreme indices from 1950 to 2003. *Journal of Geophysical Research: Atmospheres, 110*(D22).

Zhu, Lingli, Juha Suomalainen, Jingbin Liu, Juha Hyyppä, and Haggren Kaartinen. 2018. "A Review: Remote Sensing Sensors."